Investigation of the promoting effect of Mn on a Pt/C catalyst for the steam and aqueous phase reforming of glycerol

Filippo Bossola[a,b], Xavier Isidro Pereira-Hernández[c], Claudio Evangelisti[b], Yong Wang [*,c,d], Vladimiro Dal Santo [*,b]

[a] Dipartimento di Scienza e AlteTecnologie, Università dell'Insubria, Via Valleggio 11, Como, Italy, 22100.

[b] CNR - Istituto di Scienze e Tecnologie Molecolari, Via Golgi 19, Milano, Italy, 20133.

[c] The Gene and Linda Voiland School of Chemical Engineering and Bioengineering, Washington State University, Pullman, Washington 99164, United States.

[d] Institute for Integrated Catalysis, Pacific Northwest National Laboratory, Richland, Washington 99354, United States.

*Yong.Wang@pnnl.gov; v.dalsanto@istm.cnr.it

Abstract

The catalytic performances in steam reforming (SR) and aqueous phase reforming (APR) of glycerol of a bimetallic Pt-Mn catalyst supported on activated carbon are investigated and correlated with the surface properties of the catalyst. Under SR conditions, Mn showed a significant promoting effect over Pt/C, both in terms of hydrogen production rate and conversion, with a higher selectivity toward the glycerol dehydration products. Upon addition of Mn the amount of strong Lewis acid sites increased, promoting the dehydration of glycerol and favoring the C-O over C-C cleavage at expenses of hydrogen selectivity. Conversely, under APR conditions, a slightly higher hydrogen selectivity and only minimal enhancement in hydrogen production were found, whilst the products selectivity was comparable to Pt/C. Most of Mn leached into the aqueous media, but the remaining (< 5% of the fresh parent sample) might be alloyed with Pt and promote the CO desorption from neighbor Pt sites.

Keywords

Steam reforming. Aqueous phase reforming. Glycerol. Hydrogen. Platinum. Manganese. Activated carbon. Bimetallic catalyst. Surface Lewis acid site.

1. Introduction

Sustainable hydrogen production will probably play a fundamental role in future economies, due to the need of clean energy vectors to meet the modern environmental requirements, and to minimize our dependence on fossil fuels [1-4]. Water and biomass are emerging as valuable candidates to replace natural gas as main feedstock for the hydrogen production, owing to their abundance, relatively low cost, and carbon neutrality. Besides promising routes such as photoelectrochemical water-splitting and enzymatic and microbiological-based technologies, which are however in a too early stage of development for an economically sustainable implementation, reforming of biomass-derived compounds could be a viable way for the medium-term future, since it couples a well-known technology with renewable feedstocks [2-5].

In particular, steam reforming (SR) and aqueous phase reforming (APR) have been extensively studied for the past decade, showing that high hydrogen production rates can be achieved using a large variety of organic substrates, from simple model molecules to complicated mixtures, like bio-oil [3,5-13]. In this scenario, glycerol will become one of the most important commodities as it is the main byproduct from the transesterification of vegetable oils and fats to produce biodiesel, and is a good model compound for polyols in biomass catalytic conversion processes [14-16]. Many works have been published on SR and APR of glycerol for the hydrogen production, using a variety of catalysts based on both precious and non-precious metals [11,17-24]. Ru catalysts have shown good catalytic performances because of their high C-C cleavage ability and coke resistance [18], while among non-precious metals Ni is preferred [25]. However, in order to achieve good conversion levels with these catalysts, high temperatures are generally required. Pt-based catalysts can be very active even at relatively low temperature (< 300 °C), while retaining good C-C cleavage activity [25]. In order to further increasing the hydrogen production up to industrial-relevant rates, the addition of promoters is a viable strategy. Kunkes et al. had studied a series of Pt-based catalysts modified with noble and non-noble metals in the SR reaction of glycerol, and found that at low reaction temperatures only noble metals, such as Re, had a distinct promoting effect. The superior catalytic activity of the Pt-Re/C tested in that study was ascribed to a lower activation energy for CO production compared to Pt/C [24]. Besides the lack of a deeper investigation on the actual promoting mechanism, it seemed that at low temperatures only noble metals were able to promote effectively the SR of glycerol, making the development of an active non-noble metal based promoter more challenging.

To achieve that, fundamental insights on reactivity and reaction pathways can be obtained by studying the catalysts mimicking the actual working conditions. For example, an *in-operando* XAS technique was used by Dietrich et al. to study a Pt-Mo catalyst supported on carbon black for the

APR reaction of glycerol. The authors found an increased glycerol conversion, but a lower hydrogen selectivity, ascribed to the partial oxidation of Mo in APR conditions, which led to increased C-O cleavage activity through acid catalyzed reactions [21]. As one of the early effective industrial promoters used in particular for the naphtha reforming, Re has attracted much attention also for the reforming of other substrates other than glycerol, like ethylene glycol, phenols, and sugars [11,12,17,24,26]. Generally, the catalytic performances of the Pt-Re catalysts increased with all the substrates, both in SR and APR. Besides the acidity induced by the partial oxidation of Re in hydrothermal conditions, which as in the case of Mo led to higher conversion levels but lower selectivity toward hydrogen, Wang and co-workers found that the enhanced performances of Pt-Re catalysts were mostly due to the facile CO desorption from the catalyst surface by spillover from Pt to adjacent ReO_x sites, thus explaining the low activation energy for CO production found by Kunkes et al. [11,17,24,27,28].

With the aim of developing industrial-grade catalysts at lower costs, new and cheaper promoters are required. Recently, manganese has been proposed as effective promoter for Pt- and Ni-based catalysts, both in the SR and APR of oxygenates, showing remarkable performances in terms of improved hydrogen production rates [10,29]. Interestingly, Mn is an effective promoter for the CO oxidation reaction due to its good redox properties and high oxygen storage capability. This peculiar features could be useful for the production of H_2 with lower levels of CO, which is poisonous for many noble metals, and in particular Pt [30,31]. There is, however, a lack of understanding of the actual promotion mechanism of Mn in reforming reactions and about the impact of water on the bimetallic catalyst whether it is fed in the vapor or liquid phase. In this work, a Pt-Mn catalyst supported on activated carbon is studied in both SR and APR of glycerol and compared with monometallic Pt/C. The fresh catalysts were characterized by CO chemisorption, hydrogen temperature programmed reduction, HRTEM and STEM together with EDX analysis. In order to investigate the surface properties of the catalysts simulating reforming conditions with particular focus on the acidic properties, pretreatments with steam were carried out before ATR-IR with pyridine as probe molecule and NH_3-TPD experiments.

2. Experimental

2.1 Catalysts preparation

The catalysts were prepared by incipient wetness impregnation method using an activated carbon support (TA60, PICATAL) previously dried overnight at 110 °C. Tetrammineplatinum (II) nitrate hexahydrate ($(NH_3)_4Pt(NO_3)_2 \cdot 6H_2O$, Sigma-Aldrich) and manganese nitrate tetrahydrate ($Mn(NO_3)_2 \cdot 4H_2O$, Sigma-Aldrich) were used as metal precursors. The impregnated samples were

dried overnight at room temperature and calcined at 260 °C for 2 h in air. The bimetallic catalyst (Pt-Mn/C) was prepared by co-impregnation of the two metal salts, followed by the same drying and calcination steps. The Pt/Mn molar ratio was 1, with the Pt being the 2 wt.%.

2.2 Catalyst characterization

2.2.1 Physical adsorption and chemisorption

Specific surface areas were measured by nitrogen physisorption isotherms at -196 °C using the BET method (Tristar II, Micromeritics), outgassing the samples at 110 °C for 2 h before each measurement.

The metal loadings were determined by inductively coupled plasma-optical emission spectroscopy (ICP-OES) after microwave digestion of the samples in aqua regia.

CO-pulse chemisorption was performed on an Autochem II (Micromeritics). The samples were first reduced with 10 vol.% H_2/Ar at 280 °C for 1 h and then purged for 30 min with He before being cooled to 40 °C. A series of CO pulses were then introduced until saturation. Pt dispersion was evaluated by processing the thermal conductivity detector (TCD) signals, assuming a Pt/CO stoichiometry of 1.

H_2-TPR experiments were carried out on the same apparatus. Prior to each analysis, the samples were pretreated in flowing He for 1 h at 110 °C, and then cooled down to room temperature. A temperature ramp of 10 °C min^{-1} and a 10 vol.% H_2/Ar flow were used in all the experiments.

CO- and NH_3-TPD experiments were performed again by using the Autochem II (Micromeritics) apparatus. The samples were first reduced at 280 °C with a 10 vol.% H_2/Ar flow, then cooled to 225 °C under He flow. Subsequently, steam pulses were introduced for about 1 h by flowing He through a water bubbler, followed by cooling to 40 °C, and then purged for 1 h. After 1 h under CO or NH_3 flow (50 mL min^{-1}), the samples were purged with He for 1 h at room temperature. Finally, the samples were heated up with a ramp rate of 10 °C min^{-1} to 500 °C in He flow. CO desorption curves were obtained by processing the TCD signals, while the amount of desorbed NH_3 was calculated by integrating the mass signals (ThermoStar Quadropole Mass Spectrometer from Pfeiffer Vacuum).

2.2.2 Electron microscopy

Electron micrographs were carried out with a Zeiss LIBRA 200FE, equipped with: 200 kV FEG, in-column second-generation omega filter for energy selective spectroscopy (EELS) and imaging (ESI), HAADF-STEM facility and EDX probe for chemical analysis. All the samples were reduced

at 260 °C for 1 h with 10 vol.% H_2/Ar flow (50 mL min^{-1}) before performing the analyzes. Prior to the introduction in the instrument, the samples were ultrasonically dispersed in isopropyl alcohol and a drop of the suspension was deposited on a holey carbon gold grid (300 mesh). The histograms of the metal particle size distribution for the samples were obtained by counting at least 500 particles onto the micrographs. The mean particle diameter (d_m) was calculated by using the formula $d_m = \sum d_i n_i / \sum n$, where n_i is the number of particles with diameter d_i.

2.2.3 ATR-IR

Detailed ATR-IR experiments are described in our previous report [17]. The Internal Reflection Element (IRE) was coated by suspending 5 mg of catalyst in 1 mL of Milli-Q water, and sonicating the solution for 30 s. Continuously, 400 µL of solution were deposited on the surface of the IRE. Finally, the solution was dried for 1 h at 90 °C using a heating rate of 10 °C min^{-1}. The acidity of the catalyst was probed mimicking the reaction conditions, that is reduction of the catalyst followed by treatment with steam.

The procedure was as follows: 1) The ATR cell was heated to 280°C under helium at a heating rate of 5 °C min^{-1}. 2) Once at 280 °C, the catalyst was reduced by flowing 10% H_2/Ar (40 mL min^{-1}) for 30 min. 3) Residual hydrogen was removed by purging with helium for 30 min (40 mL min^{-1}). 4) The ATR cell was cooled to 225 °C, and 10 pulses of steam were injected by flowing helium into a water bubbler at room temperature in order to fill a 50 µL loop. The time between pulses was 2 min. 5) After the last pulse, the remaining steam was flushed for 30 min using helium (40 mL min^{-1}). 6) The ATR cell was cooled down to 40 °C under helium, and a background was taken. 7) 10 pulses of pyridine were injected as described in 4). 8) Spectra were collected after He purging at 40 °C. The equipment used was a Bruker Tensor 27. The resolution of the scans was 4 cm^{-1} and 128 scans were averaged for each spectrum.

2.3 Catalytic experiments

A lab-scale test unit with a fixed-bed reactor was used for the steam reforming reactions [32]. In a typical experiment, a certain amount of catalyst diluted with SiC (60-100 mesh, five times dilution in weight) was held in place by quartz wool in a quartz tube. In order to prevent condensation, both the vaporizer and the downstream line were heated with heating tape, while the low boiling-point reaction products were condensed in a cold trap at 0 °C. Before the reaction, the catalysts were reduced *in-situ* at 280 °C for 1 h with 10 vol.% H_2/Ar flow (50 mL min^{-1}), purged for 30 min with N_2 (50 mL min^{-1}), and then cooled to the reaction temperature (225 °C). A syringe pump was used to introduce a 10 wt.% glycerol/water solution using nitrogen as carrier. The gas hourly space

velocity (GHSV) was varied by adjusting the liquid and gas flow rates, keeping constant the partial pressure of the reactants. The outlet gases were dried by passing through an anhydrous $CaSO_4$ Drierite drying column, and analyzed with an online Agilent 490 micro GC with four independent modules equipped with a TCD, using nitrogen as internal standard. Aqueous phase reforming reactions were performed in a stainless-steel bench reactor (Parr 4848). Typically, a certain amount of catalyst was first reduced *ex-situ* at 280 °C for 1 h with 10 vol.% H_2/Ar flow (50 mL min^{-1}), and then transferred into the reactor containing the same reaction mixture of the steam reforming experiments. The mixture was continuously stirred at 200 rpm. The reactor was purged for 30 min with nitrogen flow and pressurized with an initial pressure of 30 bar which served also as internal standard for the quantification of the gaseous products. The reactor was then heated at 225 °C, and held at this temperature for 1 h. Finally, the reactor was cooled down to room temperature. The gaseous products were collected in an Agilent sampling gas bag (0.5 L capacity, Tedlar), and analyzed with the same Agilent 490 micro GC used for the steam reforming experiments. After depressurization, the liquid products were collected and filtered with a 0.45 μm PTFE filter. The condensed liquid products of both the SR and APR reactions were analyzed with an offline Agilent 7890A GC. The composition was calculated by external calibration curves. The equations used for the calculation of the conversion, the turnover frequency (TOF) of hydrogen, and the selectivity toward the reaction products are the following:

$$\text{Conversion (\%)} = \frac{\text{C moles in the products}}{\text{C moles in the feed}} \times 100$$

$$\text{H}_2\text{ Selectivity (\%)} = \frac{\text{H}_2\text{ moles produced}}{\text{C moles in the products} \times 7} \times 100$$

$$\text{Selectivity of } i \text{ (\%)} = \frac{i \text{ moles produced}}{\text{C moles in the products}} \times 100$$

$$\text{TOF of H}_2\left(\text{min}^{-1}\right) = \frac{\text{H}_2\text{ production rate}}{\text{Pt dispersion}}$$

3. Results

3.1 Materials characterization

The actual metal loadings of the catalysts calculated by ICP-OES are close to the target ones (i.e., 2 wt.% of Pt and 0.56 wt.% of Mn) (Table 1), except for the Mn/C catalyst where the Mn loading was found 1.79 wt.%.

The BET specific surface area of the Mn-based catalyst is similar that of the bare support, whereas the Pt-based catalysts have slightly lower values, probably due to partial pore plugging.

The Pt dispersion was evaluated by CO-pulse chemisorption, assuming a stoichiometry of CO/Pt of 1. As can be seen in Table 1, the co-impregnation procedure for the preparation of the Pt-Mn/C sample had almost no impact on the Pt dispersion, suggesting that in both the monometallic and bimetallic samples the Pt is highly dispersed (> 92%). Considering that the Mn/C sample showed no CO uptake, a simultaneous adsorption by the two metals in the bimetallic sample is unlikely.

Table 1. Metal loadings, CO uptake, Pt dispersions, and specific surface areas of the samples.

Sample	Pt (wt.%)	Mn (wt.%)	CO uptake (μmol g^{-1})*	Dispersion (%)*	SSA_{BET} (m^2 g^{-1})
C	-	-	-	-	1075
Pt/C	1.41	-	68.6	94.5	957
Pt-Mn/C	1.21	0.51	57.2	92.1	992
Mn/C	-	1.79	-	-	1093

*Calculated by CO-pulse chemisorption.

3.1.1 H_2-TPR

H_2-TPR experiments were used to investigate the effect of the addition of Mn on the reducibility of the Pt-Mn/C catalyst (Figure 1). The TPR profile of Mn/C exhibited only one weak peak centered at around 270 °C, probably due to the reduction of nonstoichiometrically dispersed MnO_x species [33,34], and a broad peak over 500 °C, which is attributed to the gasification of the support [35,36]. Pt/C showed a single and symmetric reduction peak centered at 167 °C, which corresponds to a hydrogen consumption of 0.09 mmol g^{-1}, consistent with the reduction of Pt^{+2} to Pt^0. The addition of Mn caused a shift of the reduction peak to a higher temperature (186 °C), along with an increased hydrogen consumption up to 0.15 mmol g^{-1}.

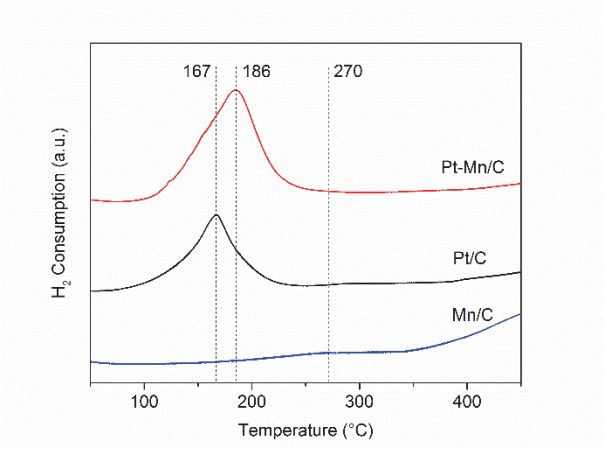

Figure 1. H_2-TPR profiles of Pt-Mn/C, Pt/C, and Mn/C.

3.2 Catalytic reactivity

3.2.1 Steam reforming

Steam reforming of glycerol over the three samples was carried out at 225 °C using a 10 wt.% aqueous solution. The product selectivity was evaluated at the same conversion level (~25%) by adjusting the GHSV. The main gaseous reaction products were H_2, CO, CO_2, and CH_4, with traces of ethylene and ethane. Besides unreacted glycerol, the liquid phase consisted mostly in ethylene glycol (EG), acetol, alcohols (methanol and ethanol), acetic acid (AcA), and acetaldehyde. The results are summarized in Table 2.

A blank test with activated carbon gave negligible activity, as well as with the Mn/C catalyst (conversion <1%). Figure 2 shows the catalytic performances of the Pt/C and Pt-Mn/C catalysts in terms of conversion and TOF of H_2. The results obtained with the Pt/C are consistent with previous studies reported in the literature [17,37], with a conversion of 26 % and a TOF of H_2 of 6 min^{-1}. As expected, CO and EG, along with the alcohols, were the main products in the gaseous and liquid phase, respectively. Addition of Mn to Pt significantly enhanced both the TOF of H_2 and the conversion, which were increased by a factor of about 3 and 4, respectively. Notably, at the same conversion level (~25%) the TOF of H_2 was 21 min^{-1}, which is about three times higher than that shown by Pt/C. Moreover, while the conversion toward gaseous products doubled, about a factor of 5 enhancement of the conversion toward liquid products was found. The presence of Mn also drastically changed the selectivity of the products, which was evaluated at comparable conversion levels (~25%). Specifically, in the gaseous products, the selectivity toward CO and H_2 dropped to from 61% to 40% and 37% to 25%, respectively, while the liquid phase consisted basically of acetol. Little difference in selectivity of CO_2 and alcohols was observed between Pt/C and Pt-Mn/C (Table 2). Although the H_2 selectivity was lower, the Pt-Mn/C showed higher conversion and TOF of H_2 compared to Pt/C.

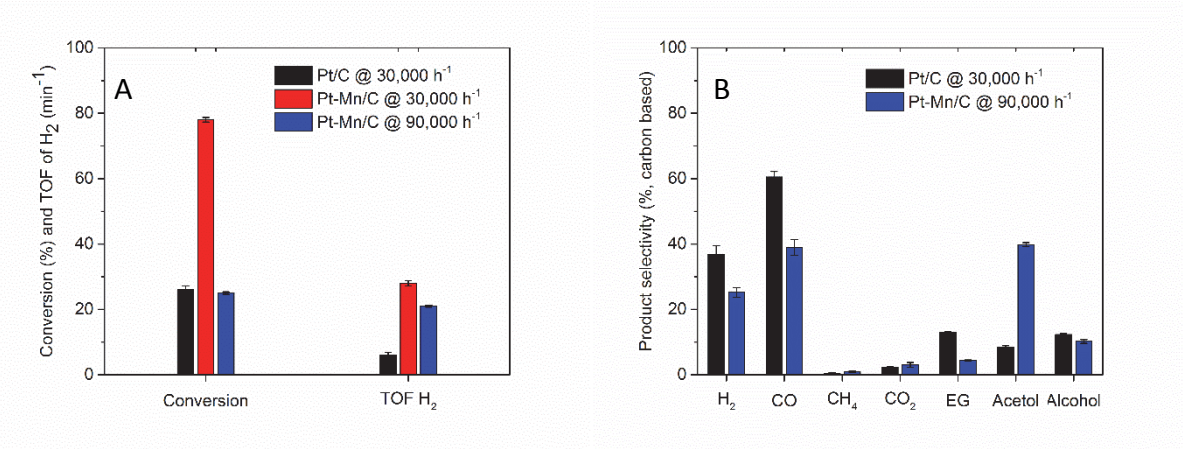

Figure 2. Conversion and TOF of H_2 of Pt/C (GHSV of 30,000 min^{-1}) and Pt-Mn/C (GHSV of 30,000 h^{-1} and 90,000 h^{-1}) in SR of 10 wt.% of glycerol aqueous solution at 225 °C (A). Product selectivity of Pt/C and Pt-Mn/C evaluated at the same conversion level (B).

Table 2. Conversion and product selectivity data of steam reforming of glycerol over Pt/C and Pt-Mn/C.

	Conversion (%)			Product selectivity (C-based, %)*								
Catalyst	Total	Gas product	Liquid Product	H_2	CO	CO_2	CH_4	EG	Acetol	Alcohols	AcA	Acetaldehyde
Pt/C	26.0	20.1	5.9	36.9	60.5	2.3	0.5	13.0	8.5	12.3	2.0	0.9
Pt-Mn/C	78.2	43.6	34.6	25.2	39.0	3.0	0.9	4.4	39.8	10.2	0.7	2.0

*Product selectivity evaluated at 30,000 h^{-1} and 90,000 h^{-1} of GHSV for Pt/C and Pt-Mn/C, respectively.

3.2.2 Aqueous phase reforming

The catalytic performances of the catalysts were evaluated in the APR of 10 wt.% glycerol at 225 °C. The reactions were carried out in a batch reactor with an initial nitrogen pressure of 30 bar. As in the case of SR, the catalytic activity of Pt/C observed is comparable to previous studies reported in the literature (Figure 3) [27,38]. The main reaction products were H_2, CO_2 and CH_4 in the gaseous phase, and ethylene glycol (EG), acetol, alcohols (methanol and ethanol), acetic acid (AcA), and acetaldehyde were collected in the liquid phase besides unreacted glycerol. In contrast with SR, the addition of Mn had a minor impact on the catalytic activity and product distribution. In particular, the conversion and TOF of H_2 were improved by a factor of 1.3 and 1.4, respectively (Table 3). Practically no difference in products selectivity was found over Pt/C and Pt-Mn/C, with the exception of the selectivity toward H_2, which increased from 51.3% to 58.0%.

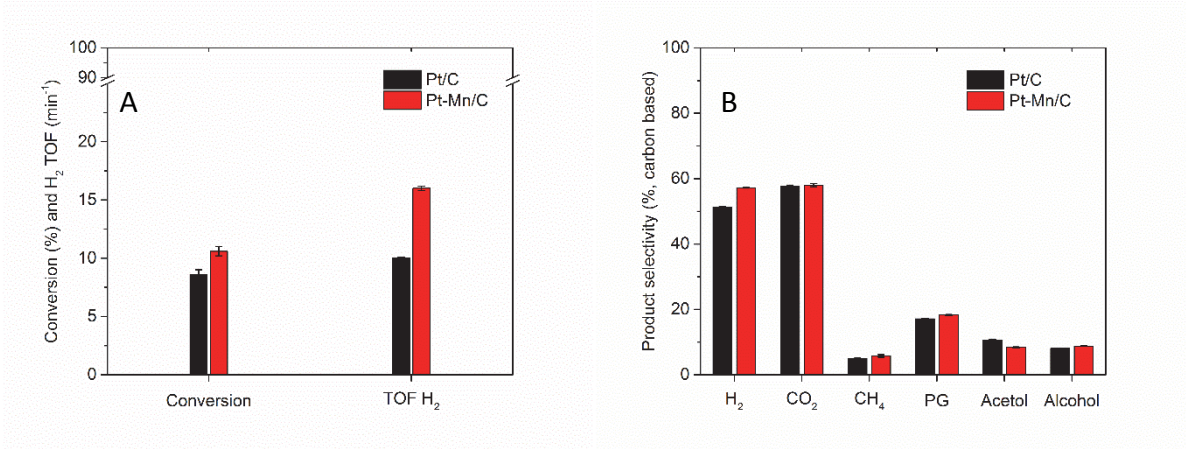

Figure 3. Conversion and TOF of H_2 (A) and product selectivity (B) of Pt/C and Pt-Mn/C in APR of 10 wt.% glycerol aqueous solution at 225 °C and 30 bar of initial pressure.

Table 3. Conversion and product selectivity data of aqueous phase reforming of glycerol over Pt/C and Pt-Mn/C.

	Conversion (%)			Product selectivity (C-based, %)							
Catalyst	Total	Gas product	Liquid Product	H_2	CO_2	CH_4	EG	Acetol	Alcohols	AcA	Acetaldehyde
Pt/C	8.6	7.6	1.0	51.3	57.7	4.9	17.1	10.7	8.3	1.0	0.3
Pt-Mn/C	10.6	9.4	1.2	58.0	58.0	5.8	18.3	8.4	8.4	0.5	0.3

3.3 Electron microscopy

The morphological and structural features of the Pt-based mono- and bimetallic catalysts were investigated by electron microscopy analyses (Figures 4,5 and S1-S4). HAADF-STEM images collected on fresh Pt/C and Pt-Mn/C showed the carbonaceous support densely populated by monodispersed metal particles with very small particle sizes (mean diameter less than 1.0 nm) in both cases (Figures 4A and 4B). STEM-EDX elemental maps of the bimetallic Pt-Mn/C catalysts revealed the presence of both Pt and Mn homogeneously dispersed all over the carbonaceous support (Figure S1). These results agree with the high Pt dispersion (> 92%) calculated by CO pulse chemisorption analysis. However, a lower amount of Mn was detected as larger aggregates mainly as MnO_2 crystalline structure (Figure S2).

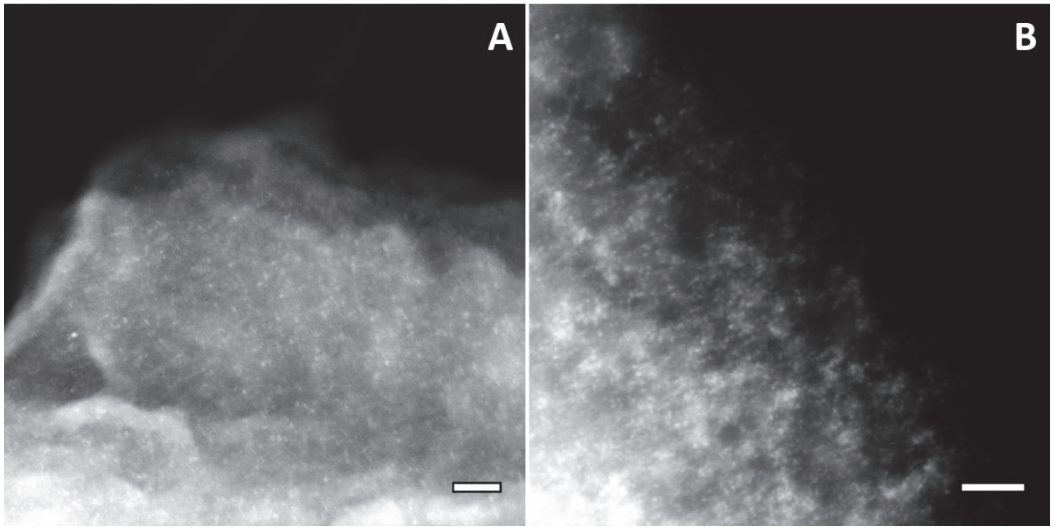

Figure 4. Representative HAADF-STEM images of Pt/C (A), Pt-Mn/C (B) (the length of the scale bar corresponds to 20 nm).

HAADF-STEM (Figure 5A) and TEM (Figure S3) analysis of the Pt-Mn/C catalyst after SR revealed the presence of Pt nanoparticles with a slightly higher mean particle size (d_m = 1.5 nm, SD = 0.4). A similar Pt nanoparticle distribution was obtained in Pt-Mn/C catalyst after APR (d_m = 1.7 nm, SD = 0.4) (HAADF-STEM, Figure 5B, and TEM, Figure S4). The analogously prepared Pt/C catalyst showed a slightly larger increase of the particle sizes both in SR (1.8 nm, SD = 0.4) and APR (d_m = 2.1, SD = 0.5).

Pt and Mn EDX signals were detected in both Pt-Mn/C after SR and after APR and compared with those registered for the fresh sample (Figure S7 and S8). However, in the post-SR sample both the signals were comparable in intensity to those found in the fresh catalyst, whereas in the post-APR sample the signal of Mn almost disappeared indicating a marked decrease of Mn content with respect to the parent fresh sample.

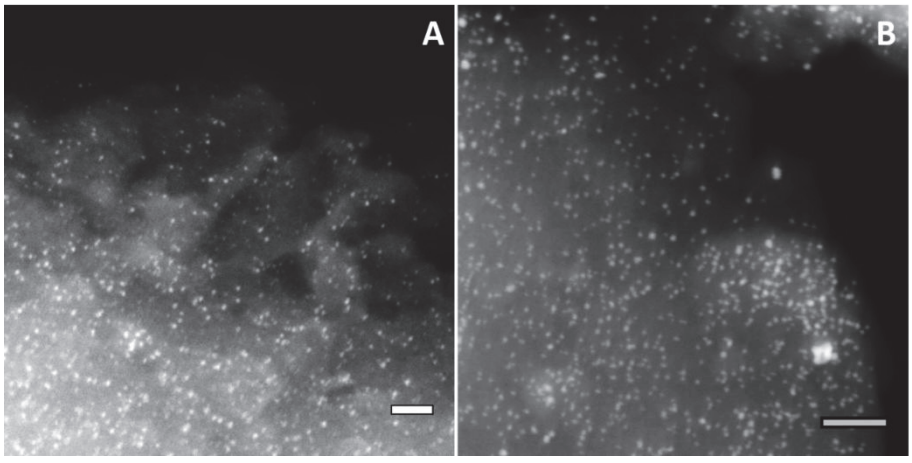

Figure 5. Representative HAADF-STEM images of Pt-Mn/C after SR (A) and APR (B) (the length of the scale bar corresponds to 20 nm).

3.4 CO- and NH_3-TPD

In order to rule out any possible effect of the CO spillover from the Pt sites promoted by Mn, as in the case of Re over Pt-Re/C [11,17], CO-TPD experiments were performed (Figure 6A). Prior to the adsorption of CO, the samples were treated with steam pulses at 225 °C to mimic the reforming conditions. Similar to CO-pulse chemisorption experiments, the Mn/C sample gave negligible CO adsorption. No significant difference was found in the CO-TPD profiles of Pt/C and Pt-Mn/C, with only one maximum at 102 °C.

The total acidity and the relative strength of the catalysts were evaluated by ammonia TPD experiments (Figure 6B). As per the CO-TPD analysis, the samples underwent the pretreatment with steam at 225 °C. A base line was established with only the activated carbon support (not shown), which gave a negligible amount of adsorbed ammonia. Both Pt/C and Mn/C catalysts exhibited similar acid strength with a singular peak centered at around 129 °C, whereas the ammonia desorption profile of Pt-Mn/C showed a peak at lower temperature (111 °C) with a shoulder at 169 °C. The total number of acid sites was calculated by integrating the desorption peaks, giving 149 μmol g^{-1} of ammonia adsorbed on Pt-Mn/C, while less acid sites were found on Pt/C and Mn/C, with 55 and 118 μmol g^{-1}, respectively.

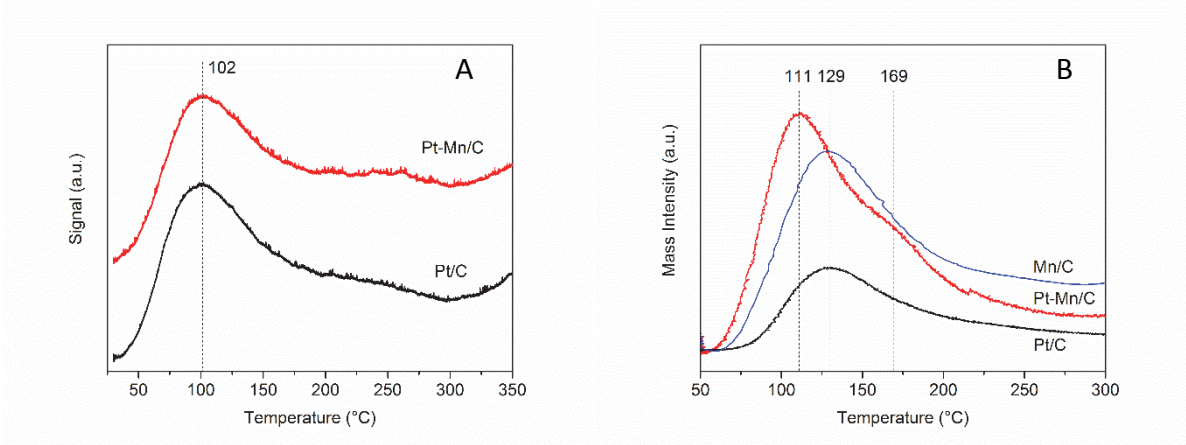

Figure 6. CO-TPD on Pt/C and Pt-Mn/C (A), and NH_3-TPD on Pt/C, Mn/C and Pt-Mn/C (B). All catalysts were reduced at 280 °C and saturated with steam at 225 °C prior to the experiments.

3.5 ATR-IR

Due to the strong IR absorption of carbon based materials, an ATR-IR technique with *in-situ* capability was used to investigate the nature of the acid sites of the catalysts. Prior to the adsorption of pyridine, the samples were reduced at 280 °C, and then treated with steam at 225 °C. All the experiments were repeated in order to make sure that the observed signals were not due to spectrum noise. Figure 7 shows the spectra obtained, while the experiment carried out with only the support gave only a background signal (not shown) [39]. The bands located in the region around 1440 and

1600 cm^{-1} are peculiar of pyridine interacting with Lewis acid sites (L), while the interaction with Brønsted acid sites (B) gives bands at 1540 and 1640 cm^{-1}. The band at 1480 $cm^{-1}$is due to the simultaneous interaction of pyridine on coupled Lewis and Brønsted acid sites [40]. Unlike Re/C, which showed no pyridine adsorption even after harsh pretreatments like with hot liquid water [11], Mn/C exhibited two broad features centered at around 1550 $cm^{-1}$and 1640 cm^{-1} that can be assigned to pyridine coordinated to Brønsted acid sites. In addition, a weak band at about 1430cm^{-1} and a shoulder at 1575 cm^{-1} are also resolved, which can be assigned to pyridine coordinated to strong Lewis acid sites [11,41]. Only Lewis type acidity was observed on Pt/C, with a clear peak resolved at 1440 cm^{-1} and a broader feature centered at around 1600 cm^{-1}, likely due coordinately unsaturated $Pt^{\delta+}$ sites. The spectrum of Pt-Mn/C resembled that of Mn/C, showing both the broad features around 1550 cm^{-1} and 1640 cm^{-1} due to protonated pyridine, and the peaks assigned to Lewis sites at 1430 $cm^{-1}$and 1575 cm^{-1}. However, the intensity of all the peaks, and particularly of those due to the Lewis acid sites, were much more intense than Mn/C.

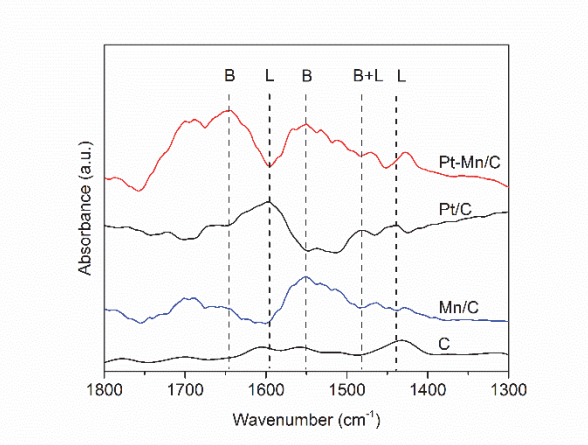

Figure 7. Pyridine adsorption on Pt-Mn/C, Pt/C, Mn/C, and carbon support investigated by ATR-IR spectroscopy (L: Lewis acid sites; B: Brønsted acid sites). All catalysts were reduced at 280 °C and saturated with steam at 225 °C prior to the experiments.

4. Discussion

One of the most important key features of supported metal catalysts for heterogeneous reactions is the metal dispersion [42]. It is generally accepted that a proper metal dispersion, as well as a sharp size distribution, must be achieved in order to maximize the catalytic performances. While not always smaller metal nanoparticles mean higher catalytic activity, like in the case of Rh nanoparticles for the methane steam reforming where particles below 2.5 nm showed fast deactivation due to coking [43], in the steam reforming of glycerol small nanoparticles of noble metals are desirable [11,17,44,45].

In the present work, Pt particles sizes homogeneously distributed below 1.0 nm in diameter (HRTEM) were obtained by simple incipient wetness impregnation in both Pt/C and Pt-Mn/C catalysts. Moreover, Pt dispersions as high as 94.5%, calculated by CO pulse chemisorption, confirmed that most of the Pt atoms are exposed, assuming completely shelled polyhedron-nanoparticles [46]. It is worth noting that the co-impregnation procedure for the preparation of Pt-Mn/C had a negligible impact on the Pt dispersion (Table 1), indicating again the presence of well dispersed Pt nanoparticles and no surface coverage by Mn-based species. The very similar Pt dispersions of Pt/C and Pt-Mn/C allows the meaningful comparison of the catalytic results, in particular concerning the TOF of H_2.

Besides dispersions, the proximity and the interaction between the two metals are critical for the activity of a bimetallic catalyst [47,48]. In the present work, an interaction of Pt with Mn, which is probably in the oxidized form since no reduction peaks were observed in the H_2-TPR profile of Mn/C below 300 °C, can be reasonably inferred by the presence of a unique reduction peak at a higher temperature than that of Pt/C (Figure 1). Moreover, if assuming that the average oxidation state of Pt remains unchanged, it has already been reported that the almost double hydrogen consumption shown by Pt-Mn/C compared to Pt/C is due to Pt nanoparticles interacting with well dispersed MnO_x centers [30]. A further evidence of the proximity of the two metals comes from the EDX maps (Figures S1) that show a homogeneous distribution of the two metals, with the signals of Pt and Mn always homogeneously covering the entire surface of the catalyst. Another key point in a bimetallic catalyst is the ratio between the two metals.

In this work, a Pt to Mn molar ratio of 1 was chosen according to the work by Kim *et al.*, where among a series of Pt-Mn catalysts tested in the APR of ethylene glycol, the molar ratio of 1 showed the highest catalytic activity both in terms of hydrogen production rates and carbon conversion. The different Pt precursor ($H_2PtCl_6{\cdot}6H_2O$) and the higher reduction temperature (350 °C) used in that study resulted in a low Pt dispersion (43.0%) and, more importantly, in the formation of a bulk alloy between Pt and Mn as revealed by the peak at 40.3° in the X-ray diffraction (XRD) pattern, attributed to Pt alloyed in bulk [10]. The very small Pt nanoparticles size achieved in this study in the Pt-Mn/C sample made impossible the resolution of any X-ray diffraction peak.

Although the Pt-Mn/C investigated in this work has many similarities with other catalysts previously described, like Pt-Re/C, its reactivity in SR and APR presents some differences, probably owing to the presence of Mn in the oxidized form. All the catalytic tests were performed with a 10 wt.% of glycerol at 225 °C. In the SR, the Pt/C catalyst exhibited catalytic performances in both the reactions in line with previous works at comparable experimental conditions, with a

TOF of H_2 of about 6 min^{-1} [17,25,27]. The main reaction products were, as expected, mainly due to reaction pathways where the C-C bonds cleavage is favored, such as ethylene glycol in the liquid phase, with only a minor part of products derived by the scission of the C-O bonds, like acetol [49]. The low amount of carbon dioxide produced in the SR reaction is due to the poor water gas shift activity of Pt supported on carbon even at relatively low temperatures [50]. The addition of Mn to Pt/C catalyst had a different impact on the catalytic performances of SR with respect to APR of glycerol. In fact, in the first case, the Pt-Mn/C catalyst showed improved TOF of H_2 and glycerol conversion of about factors of 3 and 4, respectively. Conversely, only a slight increase in hydrogen production and conversion was found in the APR reaction.

A careful analysis of the reaction products, which are correlated to the reaction pathway, may provide insights on the improved catalytic activity of Pt-Mn/C in SR of glycerol. As shown in Table 2, while the conversion of Pt/C was prevalently directed toward the gaseous products. Besides the increase of the overall conversion, with Pt-Mn/C the formation of liquid products was more favored, in particular towards acetol, which is formed by dehydration of glycerol, reflecting the higher selectivity toward C-O bond cleavage of the catalyst. Moreover, the preferred dehydration pathway followed by Pt-Mn/C is evidenced by the lower selectivity toward hydrogen and carbon monoxide, which are formed by dehydrogenation followed by decarbonylation of glycerol, as in the case of Pt/C (Table 2). Ethanol and methanol can be formed via both pathways as final products of the dehydrogenation of ethylene glycol or acetol, therefore they are less indicative of the reaction pathway followed by the catalysts [17,27].

The different reaction pathways proceeded on Pt/C and Pt-Mn/C in the SR of glycerol can be explained by the higher acidity of the Mn-promoted catalyst, while is less likely a mechanism involving CO spillover from Pt sites to MnO_x because otherwise differences in the product selectivity should have been observed [17,27]. However, in order to rule out any possible CO spillover effect, CO-TPD experiments were carried out pretreating the samples with steam at 225 °C to simulate SR conditions. As expected, no difference in the desorption profiles were found, with both Pt/C and Pt-Mn/C showing a singular desorption peak centered at 102 °C (Figure 6A). The same pretreatment was used in the NH_3-TPD experiments to investigate the acid character of the samples again simulating SR conditions. Based on the location of the desorption peaks, Pt/C and Mn/C had the same acid strength. This is in accordance with several authors who had reported similar results on similar systems, showing that, compared to more classical acidic materials like silica-alumina, supported Mn oxides catalysts have generally rather low acid strength, due to both Lewis- and Brønsted-type sites [51-53].

A thorough investigation of the nature of the acid sites present in all the catalysts was made possible using an *in-situ* ATR-IR technique with pyridine as probe molecule. Pt/C showed only Lewis-type acidity, as revealed by the peaks resolved at 1599 cm^{-1} and 1440 cm^{-1}, probably due to electron deficient $Pt^{\delta+}$ centers formed as consequence of the steam pretreatment. As expected, both Lewis and Brønsted acid sites were present in Mn/C, with the broad feature centered at 1550 cm^{-1} ascribed to protonated pyridine, suggesting a prevalence of Brønsted sites in this sample (Figure 7) [30]. Noteworthy, two barely resolved bands centered at lower frequency than those assigned to Lewis acid sites in Pt/C were observed, indicating the presence of strong Lewis-type acidity [11]. These strong sites were probably too few in number to be revealed and then quantified by the NH_3-TPD. After adding Mn to Pt, a shoulder at high temperature was observed in the ammonia desorption profiles, along with a shift to a lower temperature of the main reduction peak. In addition, in the ATR-IR spectrum of Pt-Mn/C the bands assigned to strong Lewis acid sites increased in intensity (Figure 7). Since the same low-frequency peaks, although very weak, were also found in Mn/C, they can be reasonably assigned to exposed $Mn^{\delta+}$ centers. As suggested by the H_2-TPR experiments (Figure 1), where Pt-Mn/C showed a higher hydrogen consumed than Pt/C, the increased number of strong Lewis acid sites could be the result of the interaction between the two metals [38]. It has been recently demonstrated that the increased formation of acid-catalyzed products in the reforming of glycerol, like acetol, is indeed due to the presence of strong Lewis acid sites [11,54-56]. However, the negligible catalytic activity of Mn/C indicates that the activation of glycerol initiates on the Pt sites, and then proceeds towards acid-catalyzed reactions on exposed oxidized $Mn^{\delta+}$ sites, shifting the product selectivity toward acetol. Brønsted acid sites on Pt-Mn/C, whose presence was evidenced by the broad feature at 1599 cm^{-1}, seemed to have minor influence on the reaction, since no products derived by proton-catalyzed reaction were found [56]. The retained selectivity toward CO_2 with respect to Pt/C is probably due to the CO oxidation capability of Mn oxides [30]. In conclusion, the higher hydrogen productivity shown by the bimetallic Pt-Mn/C catalysts is not strictly due to the higher glycerol conversion. Rather, the few, strong Lewis acid sites generated by $Mn^{\delta+}$ participate to the activation of the glycerol molecules on the neighbor Pt sites. Subsequently, these activated glycerol molecules undergo reforming reaction more easily than with the conventional monometallic Pt-based catalyst, eventually leading to much higher hydrogen production rates.

As far as the APR reactions is concerned, Pt-Mn/C and Pt/C showed similar catalytic performances, as well as the same products selectivity. A moderately higher TOF of H_2 and conversion level with 1.4 and 1.3 enhancement factors, respectively, were shown by Pt-Mn/C. ICP-OES analysis on used Pt-Mn/C revealed that most of all the Mn leached out from the catalyst, thus

explaining the similarity with Pt/C, in particular in terms of products selectivity. The lower amount of Mn was also confirmed by EDX analysis (Figure S3). Wang and co-workers had studied similar systems (i.e., Pt-Re/C) for APR reactions, and found that although around 50% of Re leached out, the catalyst retained its superior catalytic activity compared to Pt/C. The presence of both oxidized Re and an alloy between Pt and Re was revealed by *in-situ* XPS and Raman measurements [27]. Similarly, the formation of an alloy between Pt and Mn in the Pt-Mn/C catalyst studied by Kim *et al*. in the APR of ethylene glycol was evidenced by XRD analysis, and attributed for the increased activity [10]. Comparable conclusions were also formulated by Dietrich et al. for a Pt-Mo catalyst in the APR of glycerol [21]. It appears that the enhanced reforming performances of a bimetallic catalyst in APR reactions is related to the presence of an alloy between the noble metal and the promoter, stabilizing the latter against dissolution. In the Pt-Mn/C investigated in this study, the amount of Pt alloyed with Mn was reasonably considered negligible, or at least not enough to have a major impact on the reactivity. The slightly improved TOF and selectivity of H_2 might be explained by the presence of a small amount of Mn alloyed with Pt that did not leach into the reactant solution, and by considering a promotional mechanism similar to that reported for Pt-Re/C catalyst (vide supra). Indeed, ICP-OES analysis on the spent catalyst revealed a residual presence of Mn (<5% of the fresh sample). Contrary to APR, neither Pt nor Mn loss was evidenced on the spent Pt-Mn/C used in the SR. EDX analysis on the post-SR and post-APR samples (Figure S7 and S8, respectively), compared to the ones of the fresh samples, confirmed the ICP-OES results.

5. Conclusions

The catalytic performances of a bimetallic Pt-Mn/C catalyst were investigated in the SR and APR of glycerol. In the first case, with water fed as steam, the catalyst showed enhanced TOF of H_2 and conversion compared to Pt/C, whereas with liquid water only a slight improvement was found. In SR, upon addition of Mn, the product selectivity shifted toward acetol at expense of CO and H_2, indicating that the dehydration of glycerol (that is the C-O bond scission) was more favored than the dehydrogenation pathway (that is the C-C bond scission). This behavior could be ascribed to the increased acidity of Pt-Mn/C, and in particular to the presence of few strong Lewis acid sites, which promote the activation of the glycerol molecules on the Pt sites, leading to both remarkable higher hydrogen productivity and increased selectivity toward acid-catalyzed products. In APR conditions most of the Mn leached into the reactant solution, but the residual metal still present on the catalyst might be responsible for the slight increase in catalytic activity, suggesting that an alloy formation might be fundamental for the stabilization of the promoter under such harsh reaction conditions.

6. Acknowledgements

We acknowledge the financial support from the US Department of Energy (DOE), Office of Basic Energy Sciences, Division of Chemical Sciences, Geosciences, and Biosciences under the award number DE-AC05-RL01830 (FWP-47319) for Y.W. and DE-FG02-05ER15712 for F.B. and X.I.P.H.

7. References

[1] G. Marbán, T. Valdés-Solís, Int. J. Hydrogen Energ., 32 (2007) 1625-1637.

[2] S.E. Hosseini, M.A. Wahid, Renew. Sust. Energ. Rev., 57 (2016) 850-866.

[3] J.D. Holladay, J. Hu, D.L. King, Y. Wang, Catal. Today, 139 (2009) 244-260.

[4] N. Armaroli, V. Balzani, ChemSusChem, 4 (2011) 21-36.

[5] R.D. Cortright, R.R. Davda, J.A. Dumesic, Nature, 418 (2002) 964-967.

[6] S.D. Davidson, H. Zhang, J. Sun, Y. Wang, Dalton Trans., 43 (2014) 11782-11802.

[7] R. Trane-Restrup, D.E. Resasco, A.D. Jensen, Catal. Sci. Technol., 3 (2013) 3292.

[8] R. Trane, S. Dahl, M.S. Skjøth-Rasmussen, A.D. Jensen, Int. J. Hydrogen Energ., 37 (2012) 6447-6472.

[9] R.M. Navarro, R. Guil-Lopez, A.A. Ismail, S.A. Al-Sayari, J.L.G. Fierro, Catal. Today, 242 (2015) 60-70.

[10] H.-D. Kim, H.J. Park, T.-W. Kim, K.-E. Jeong, H.-J. Chae, S.-Y. Jeong, C.-H. Lee, C.-U. Kim, Int. J. Hydrogen Energ., 37 (2012) 8310-8317.

[11] Z. Wei, A. Karim, Y. Li, Y. Wang, ACS Catal., 5 (2015) 7312-7320.

[12] A.V. Kirilin, A.V. Tokarev, H. Manyar, C. Hardacre, T. Salmi, J.P. Mikkola, D.Y. Murzin, Catal. Today, 223 (2014) 97-107.

[13] D.J.M. de Vlieger, L. Lefferts, K. Seshan, Green Chem., 16 (2014) 864.

[14] C.A.G. Quispe, C.J.R. Coronado, J.A. Carvalho Jr, Renew. Sust. Energ. Rev., 27 (2013) 475-493.

[15] R.R. Soares, D.A. Simonetti, J.A. Dumesic, Angew. Chem. Int. Ed., 45 (2006) 3982-3985.

[16] A. Corma, S. Iborra, A. Velty, Chem. Rev., 107 (2007) 2411-2502.

[17] Z. Wei, A.M. Karim, Y. Li, D.L. King, Y. Wang, J. Catal., 322 (2015) 49-59.

[18] A. Gallo, C. Pirovano, P. Ferrini, M. Marelli, R. Psaro, S. Santangelo, G. Faggio, V. Dal Santo, Appl. Catal. B: Environ., 121-122 (2012) 40-49.

[19] A. Gallo, C. Pirovano, M. Marelli, R. Psaro, V. Dal Santo, Chem. Vapor Deposition, 16 (2010) 305-310.

524 [20] A. Iriondo, V.L. Barrio, J.F. Cambra, P.L. Arias, M.B. Güemez, R.M. Navarro, M.C. Sanchez-
525 Sanchez, J.L.G. Fierro, Cat. Commun., 10 (2009) 1275-1278.
526 [21] P.J. Dietrich, R.J. Lobo-Lapidus, T. Wu, A. Sumer, M.C. Akatay, B.R. Fingland, N. Guo, J.A.
527 Dumesic, C.L. Marshall, E. Stach, J. Jellinek, W.N. Delgass, F.H. Ribeiro, J.T. Miller, Top. Catal.,
528 55 (2012) 53-69.
529 [22] A. Iriondo, J.F. Cambra, V.L. Barrio, M.B. Guemez, P.L. Arias, M.C. Sanchez-Sanchez, R.M.
530 Navarro, J.L.G. Fierro, Appl. Catal. B: Environ., (2011).
531 [23] P.V. Tuza, R.L. Manfro, N.F.P. Ribeiro, M.M.V.M. Souza, Renew. Energ., 50 (2013) 408-414.
532 [24] P.D. Vaidya, A.E. Rodrigues, Chem. Eng. Technol., 32 (2009) 1463-1469.
533 [25] E.L. Kunkes, R.R. Soares, D.A. Simonetti, J.A. Dumesic, Appl. Catal. B: Environ., 90 (2009)
534 693-698.
535 [26] V. Stijepovic, P. Linke, S. Alnouri, M. Kijevcanin, A. Grujic, M. Stijepovic, Int. J. Hydrogen
536 Energ., 37 (2012) 11772-11784.
537 [27] L. Zhang, A.M. Karim, M.H. Engelhard, Z. Wei, D.L. King, Y. Wang, J. Catal., 287 (2012)
538 37-43.
539 [28] A.M. Karim, C. Howard, B. Roberts, L. Kovarik, L. Zhang, D.L. King, Y. Wang, ACS Catal.,
540 2 (2012) 2387-2394.
541 [29] M. Koike, C. Ishikawa, D. Li, L. Wang, Y. Nakagawa, K. Tomishige, Fuel, 103 (2013) 122-
542 129.
543 [30] J.L. Ayastuy, M.P. González-Marcos, J.R. González-Velasco, M.A. Gutiérrez-Ortiz, Appl.
544 Catal. B: Environ., 70 (2007) 532-541.
545 [31] K. Liu, C. Song, V. Subramani, Hydrogen and syngas production and purification
546 technologies, Wiley2009.
547 [32] Y. Li, Z. Wei, J. Sun, F. Gao, C.H.F. Peden, Y. Wang, J. Phys. Chem. C, 117 (2013) 5722-
548 5729.
549 [33] D. Döbber, D. Kießling, W. Schmitz, G. Wendt, Appl. Catal. B: Environ., 52 (2004) 135-143.
550 [34] F. Arena, T. Torre, C. Raimondo, A. Parmaliana, Phys. Chem. Chem. Phys., 3 (2001) 1911-
551 1917.
552 [35] D. Simonetti, E. Kunkes, J. Dumesic, J. Catal., 247 (2007) 298-306.
553 [36] M.A. Fraga, E. Jordão, M.J. Mendes, M.M.A. Freitas, J.L. Faria, J.L. Figueiredo, J. Catal., 209
554 (2002) 355-364.
555 [37] F. Pompeo, G. Santori, N.N. Nichio, Int. J. Hydrogen Energ., 35 (2010) 8912-8920.
556 [38] D.L. King, L. Zhang, G. Xia, A.M. Karim, D.J. Heldebrant, X. Wang, T. Peterson, Y. Wang,
557 Appl. Catal. B: Environ., 99 (2010) 206-213.

[39] J. Zawadziki, Carbon, 26 (1988) 627-633.
[40] G. Busca, Catal. Today, 41 (1998) 191-206.
[41] J. Sun, R.A. Baylon, C. Liu, D. Mei, K.J. Martin, P. Venkitasubramanian, Y. Wang, J. Am. Chem. Soc., 138 (2016) 507-517.
[42] N. Musselwhite, G.A. Somorjai, Top. Catal., 56 (2013) 1277-1283.
[43] D.A.J.M. Ligthart, R.A. van Santen, E.J.M. Hensen, J. Catal., 280 (2011) 206-220.
[44] F. Bossola, C. Evangelisti, M. Allieta, R. Psaro, S. Recchia, V. Dal Santo, Appl. Catal. B: Environ., 181 (2016) 599-611.
[45] W. Yu, M.D. Porosoff, J.G. Chen, Chem. Rev., 112 (2012) 5780-5817.
[46] K. An, G.A. Somorjai, ChemCatChem, 4 (2012) 1512-1524.
[47] Z. Wei, J. Sun, Y. Li, A.K. Datye, Y. Wang, Chem. Soc. Rev., 41 (2012) 7994-8008.
[48] V. Dal Santo, A. Gallo, A. Naldoni, M. Guidotti, R. Psaro, Catal. Today, 197 (2012) 190-205.
[49] A. Wawrzetz, B. Peng, A. Hrabar, A. Jentys, A.A. Lemonidou, J.A. Lercher, J. Catal., 269 (2010) 411-420.
[50] R. Buitrago, J. Ruiz-Martínez, J. Silvestre-Albero, A. Sepúlveda-Escribano, F. Rodríguez-Reinoso, Catal. Today, 180 (2012) 19-24.
[51] E. Fernández López, V. Sánchez Escribano, C. Resini, J.M. Gallardo-Amores, G. Busca, Appl. Catal. B: Environ., 29 (2001) 251-261.
[52] E. Finocchio, G. Busca, Catal. Today, 70 (2001) 213-225.
[53] F. Hao, J. Zhong, P.-L. Liu, K.-Y. You, C. Wei, H.-J. Liu, H.-A. Luo, J. Mol. Catal. A: Chem., 351 (2011) 210-216.
[54] J.R. Copeland, I.A. Santillan, S.M. Schimming, J.L. Ewbank, C. Sievers, J. Phys. Chem. C, 117 (2013) 21413-21425.
[55] G.S. Foo, D. Wei, D.S. Sholl, C. Sievers, ACS Catal., 4 (2014) 3180-3192.
[56] B. Katryniok, S. Paul, F. Dumeignil, ACS Catal., 3 (2013) 1819-1834.

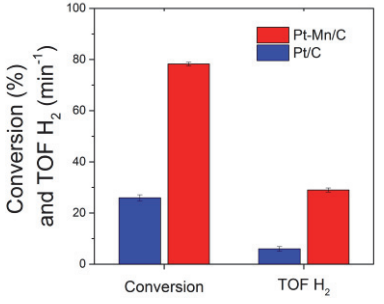
Conversion (%) and TOF H_2 (min^{-1})
100
80
60
40
20
0
Pt-Mn/C
Pt/C
Conversion
TOF H_2

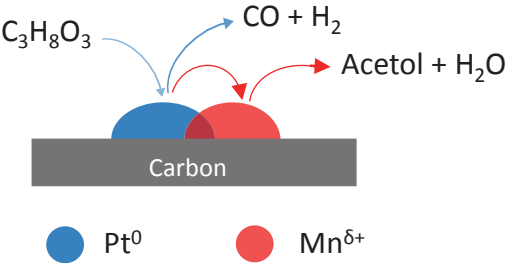
$C_3H_8O_3$
CO + H_2
Acetol + H_2O
Carbon
Pt^0
$Mn^{\delta+}$